

Abstract

Multiple studies have reported either isotropic or trapped pitch angle distributions of high energy (> 100 eV) electrons on closed crustal field lines on the dayside of Mars. These pitch angle distributions are not to be expected from collisional scattering and conservation of adiabatic invariants alone. We use two years of data from the Mars Atmosphere and Volatile Evolution (MAVEN) mission to analyze the pitch angle distributions of superthermal electrons on dayside closed crustal magnetic fields and compare to results from an electron transport model. Low energy electrons (10-60 eV) have pitch angle distributions in agreement with modeling results, while high energy electrons (100-500 eV) do not. High energy electrons have a flux peak at perpendicular pitch angles which suggests there is a ubiquitous energization process occurring on crustal fields. Wave-particle interactions seem to be the most likely candidate. Trapping of high energy electrons may impact the nightside ionosphere dynamics.

Plain Language Summary

Superthermal electrons are electrons with energies between 1-1000 eV and can be produced from ionizing a neutral atmospheric molecule (photoelectron). These electrons are efficient at shifting energy around in space environments due to their high speeds and their ability to interact with the more ubiquitous lower energy (thermal) plasma. Past studies have investigated the distribution of photoelectrons on the crustal magnetic fields of Mars and they do not always agree with past modeling results and a basic understanding of electron transport. In this study, we use data from the Mars Atmosphere and Volatile Evolution (MAVEN) mission in order to understand the distribution of these electrons throughout the Mars space environment, previously impossible due to spacecraft orbits. We find that the lower energy electrons (10-60 eV) behave as expected but the higher energy electrons (100-500 eV) do not. We find that the type of distribution statistically seen by MAVEN for these high energy electrons suggests that a ubiquitous energization process is occurring on the dayside crustal magnetic fields of Mars. We consider multiple physical processes capable of producing such observed distributions and conclude that wave-particle interactions are the most likely candidate.

1 Introduction/Motivation

Superthermal electrons (1-1000 eV) are an important population of particles common throughout the solar system. They are excellent at shifting energy from one place to another in space environments through interactions with the bulk thermal plasma. Photoelectrons are one population of superthermal electrons, produced through ionization of neutral particles, and have been studied extensively at Earth, Mars, Venus and even moons such as Titan (see Coates et al. (2011) for a review). Photoelectrons have a distinct energy spectrum that allows them to be readily identified in the data. One characteristic of the photoelectron energy spectrum include flux peaks in the 20-30 eV range determined by the dominant atmospheric neutrals. At Mars, the primary peaks occur at 22.29 eV (O) and at 22.69 and 27.02 eV (CO₂). Other unique features of the photoelectron energy spectrum at Mars include the “photoelectron knee” at ~ 60 eV as a result in a drop in ionizing solar radiation (a characteristic shared by photoelectrons at other solar system bodies as well), a flux peak due to carbon Auger electrons at ~ 250 eV visible in measurements during times of intense photoelectron fluxes (Xu et al., 2018), and another flux peak at 500 eV due to oxygen Auger electrons. These distinct spectral features have allowed studies of the Mars space environment such as Xu et al. (2014), Shane et al. (2016), and Xu et al. (2017) to determine whether a measurement is observing photoelectrons or solar wind electrons.

Pitch angle distributions (PADs) (Brain et al., 2007; Weber et al., 2017) and energy spectra (Frahm, Winningham, et al., 2006; Liemohn et al., 2006, 2006; Frahm, Sharber, et al., 2006) of superthermal electrons can be used to infer magnetic topology. More recently, Xu et al. (2017, 2019) have utilized both to more accurately determine the magnetic topology in the Mars space environment. Liemohn et al. (2003) used a superthermal electron transport model (Khazanov et al., 1993; Khazanov & Liemohn, 1995; Xu & Liemohn, 2015) to perform data-model comparisons with Mars Global Surveyor (MGS) observations, and at low energies (< 100 eV), the model-calculated PADs agreed with MGS results. However, MGS measured isotropic PADs for electrons with > 100 eV, while the model calculated a source cone PAD at these energies. This was a case study comparison, and it demonstrated that the model is missing a physical process that produced the observed MGS measurement. Brain et al. (2007) performed a statistical study of 115 eV PADs with MGS data and found that on the dayside, isotropic and trapped (2-sided loss cone) distributions are common on closed crustal field lines, in agreement with the case study of Liemohn et al. (2003). It should be noted that Brain et al. (2007) was using pitch angle distributions to classify magnetic topology, however a source cone distribution was not among the common distributions used to do so. In fact they reported that only 2.8% of the pitch angle distributions they used on the dayside had a 2-sided source cone. These studies suggest that there are unstudied physical processes producing isotropic and trapped distributions on closed crustal field lines, as conservation of adiabatic invariants and collisional scattering predicts a source cone distribution. More recently Soobiah et al. (2014) observed field aligned low energy electrons and trapped high energy electrons inside of an ionospheric flux rope and during times of radial field lines, with low energy pitch angle distributions that indicate they are open. The electron impact ionization cross sections for the primary upper atmosphere neutral species, CO_2 and O , peak around 100 eV (Thompson et al., 1995; Itikawa, 2002). Therefore, any pitch angle scattering or energy diffusion affecting electrons at these energies will affect the ionosphere below.

The work done by Liemohn et al. (2003) revealed the need to study the pitch angle distributions of superthermal electrons on closed field lines at Mars. Brain et al. (2007) furthered this need by reporting the dominant PAD on dayside closed crustal fields for electrons with 115 eV were isotropic and trapped distributions. However, the Brain et al. (2007) study used MGS data which was locked in an orbit at roughly 400 km and 2am/pm local time. This study takes advantage of the precessing elliptical orbit of the Mars Atmosphere and Volatile EvolutioN (MAVEN) mission (Jakosky et al., 2015) which allows sampling of the different regions of the Martian space environment in order to better understand the physics that control the superthermal electron PADs on dayside closed crustal field lines.

2 Data & Filtering

Over two years of data collected from the Solar Wind Electron Analyzer (SWEA) (Mitchell et al., 2016) and Magnetometer (MAG) (Connerney et al., 2015) spanning the time range 01 December 2014 - 30 December 2016 are used in this study to obtain a clearer picture of the behavior of photoelectrons on dayside closed crustal field lines. Each pitch angle distribution (PAD) is mapped onto a common pitch angle grid of 18 bins each with bin width of 10° . We limit ourselves to energies below 500 eV as there are few photoelectrons with energies greater than this.

Modified pitch angles (Xu et al., 2014; Shane et al., 2016) are used to provide more information about the direction that the electrons are traveling, specifically if the electrons are directed toward or away from the planet. If the magnetic elevation angle is greater than zero, the pitch angles are flipped (i.e. modified pitch angle = $180^\circ - \text{pitch angle}$, if $B_{elev} > 0$). Electrons with modified pitch angles of 0° - 90° have some guiding-center ve-

114 locity component in the direction of the planet, and electrons with modified pitch an-
 115 gles of 90° - 180° have some guiding center velocity component directed away from the planet.

116 In order to ensure that the measurements being used are observing electrons on day-
 117 side closed field lines and not other field line topographies, multiple filtering criteria are
 118 enforced. First, a lower altitude limit is set to 200 km to only include measurements above
 119 the photoelectron exobase where the electrons are magnetized (Xu et al., 2016). Secondly,
 120 the solar zenith angle is required to be less than 90° to include only dayside observations.
 121 We also require that the shape parameter (Xu et al., 2017) in both source cones is re-
 122 quired to be less than one. This criterion is used to filter for closed crustal magnetic fields
 123 by examining the low energy (20-80 eV) and field aligned (0-30, 150-180 pitch angle) elec-
 124 tron energy spectrum. No information of higher energy electrons and those with perpen-
 125 dicular pitch angles is used. However, this only indicates that the "ends" of the mag-
 126 netic field lie below the superthermal electron exobase. While this is true for all closed
 127 crustal field structures, draped field lines deeply embedded in the ionosphere may also
 128 share this characteristic. Therefore a fourth criteria is set that the magnetic field mag-
 129 nitude must be greater than 20 nT to attempt to avoid this scenario. This is by no means
 130 a perfect filter, but a higher threshold would start to exclude crustal fields. Lastly, to
 131 avoid spacecraft potential issues, a filter is set to only include data when the spacecraft
 132 potential (calculated using publicly available MAVEN software) is between -1V and +3V.
 133 After filtering, the dataset includes $\sim 296,000$ PAD observations each with accompany-
 134 ing magnetic field and ephemeris information.

135 **3 Expected Distribution with only Collisional Scattering - Model Re-** 136 **sults**

137 A superthermal electron transport model (STET) (Khazanov et al., 1993; Khaz-
 138 anov & Liemohn, 1995; Liemohn et al., 2003; Xu & Liemohn, 2015) is utilized to demon-
 139 strate the expected dayside superthermal photoelectron distribution on a closed dipole-
 140 like symmetric crustal field line with collisions as the only scattering process. The types
 141 of collisions included in the model are collisions with thermal electrons and ions, elas-
 142 tic collisions with neutrals, inelastic excitation scattering with neutrals, and inelastic ion-
 143 ization scattering with neutrals. Figure 1 shows the PADs of superthermal electrons at
 144 multiple locations along a field line at 45° solar zenith angle: (1a): near the superther-
 145 mal electron exobase, (1b): a position well above the exobase, and (1c): at the top of
 146 the field line. Below and near the exobase, collisions dominate and electrons are isotropic
 147 in pitch angle regardless of energy (1a). Above the exobase, the electrons are magnetized
 148 and collisions play a reducing role as the altitude increases. Collision frequencies (Coulomb
 149 and elastic collisions with neutrals) are proportional to E^{-2} where E is the energy of
 150 the electron, and this effect can be seen in 1b and more noticeably in 1c. It is easier to
 151 see in 1c because the more pronounced source cone allows any scattering into the trapped
 152 region to be more noticeable. As an electron travels up the field line, the magnetic field
 153 strength decreases. In order to conserve the first adiabatic invariant, the pitch angle of
 154 the electron becomes more field aligned producing the anisotropy seen in 1b and 1c. Fig-
 155 ure 1d plots the normalized pitch angle distribution for photoelectrons with $E = 50$ eV
 156 at each altitude (vertical slices at 50 eV through each plot). The source cone is more pro-
 157 nounced as altitude increases, i.e. the ratio of field aligned flux to perpendicular flux in-
 158 creases with altitude. This is due to the combined effects of adiabatic invariant conser-
 159 vation and the insignificance of collisions at high altitudes. Different energy electrons will
 160 have the same trend in altitude, and higher energy electrons will experience more anisotropy
 161 as collisional effects are less important. The y-axis scale used here in Fig 1d is chosen
 162 to match the rest of this paper for easier comparison. The normalized flux value at pitch
 163 angle = 90° and at altitude = 500 km drops to 0.0025.

164 Note that these PADs will change with solar conditions, atmospheric densities, and/or
 165 magnetic field configurations. The specific magnetic field strengths and background ther-

mal electron densities used are given above each subplot. Different solar conditions and atmospheric densities will move the location of the exobase, affecting where collisions play an important role in controlling the PADs of photoelectrons. Altering the magnetic field configuration may have multiple effects. The ratio of B_{local} and $B_{exobase}$ determines the size of the source cone at any given location along the field line. A field line that is longer horizontally will force electrons to travel longer distances through high density parts of the atmosphere allowing for more collisions. However, none of these changes will affect the trends in altitude or energy described above. Only the magnitude of the fluxes will be changed and the degree to which the PADs evolve in altitude/energy. We will use this representative example as a baseline and any deviation seen in the data implies missing physics in the model, and a lack of understanding of the Martian space environment.

4 Statistical Results

4.1 Energy Dependence

Figure 2 shows the average normalized pitch angle distribution over the two year filtered dataset for low energies (10-60 eV, 2a), and high energies (100-500 eV, 2b). Each curve in Figure 2 is normalized by the average flux in that energy channel over the two year period. Both measurement and statistical errors are accounted for, but due to the large sample size, these errors are small and within the circle markers. The dichotomy between low and high energies is evident from the figure. Low energy photoelectrons, on average, have a source cone distribution. From Section 3, this is what we would expect on a closed crustal field line with only collisional scattering. STET predicts that high energy photoelectrons should have a more pronounced source cone distribution. Instead, the high energy photoelectrons measured by MAVEN have a peak in flux at perpendicular pitch angles. Previously, Liemohn et al. (2003) suggested an energy dependent pitch angle scattering process is responsible for producing the isotropic high energy distributions seen by MGS. These results indicate otherwise, as pitch angle scattering processes will isotropize the distribution, not produce a peak at perpendicular pitch angles. One method of forming this distribution is on the nightside of Mars as the crustal field foot points are no longer sunlit and therefore the source of electrons has been removed (loss cone distribution). The photoelectrons at field aligned pitch angles are lost first through energy transfer with the thermal population and only the trapped particles remain (Shane et al., 2016). However, we have filtered for dayside observations where the source cone is filled with photoelectrons. Therefore, there must be an energization process occurring ubiquitously in the Martian ionosphere/magnetosphere in order to produce the average distribution observed for high energy photoelectrons. Another interesting feature to note is the asymmetry about 90° pitch angle. There are more high energy electrons with a velocity component toward the planet than away from it.

4.2 Altitude Dependence

Figure 3 shows how the normalized energy-averaged pitch angle distributions change with altitude for low (3a) and high energy (3b) photoelectrons. Flux measurements in each energy channel are normalized by the average flux for that energy for all measurements in each altitude range. The energy channels are then averaged together to produce the curves shown. Low energy photoelectrons at altitudes just above the exobase (200 - 300 km) are close to being isotropic. As the altitude increases, the average pitch angle distribution of low energy photoelectrons changes from isotropic to a source cone distribution. This source cone distribution becomes more distinct the higher the altitude, in agreement with the results from Section 3. High energy photoelectrons are also close to being isotropic at low altitudes. However, there is an asymmetry about 90° with more high energy electrons that have a velocity component toward the planet. At higher altitudes, the pitch angle distribution of high energy photoelectrons becomes perpendic-

216 ularly peaked, while the ratio of perpendicular flux to field aligned flux gets larger. Ad-
217 ditionally, the asymmetry about 90° pitch angle also gets bigger the higher the altitude.
218 Of course, these statistical results combine measurements from many magnetic field lines
219 and atmospheric profiles so a binning by magnetic elevation angle was also performed
220 (results not shown) and the perpendicular peak exists on both horizontal and vertical
221 field lines. The peak is narrower and more pronounced on vertical field lines, however,
222 this can be explained by adiabatic motion.

223 5 Example PAD

224 Figure 4 plots an example MAVEN observation from 2015-05-24. These measure-
225 ments took place on the dawn side of the planet (7 local time, 77° solar zenith angle) and
226 over the strong crustal magnetic fields in the southern hemisphere (50° S, 150° E). Fig-
227 ure 4a, 4b, and 4c plot time series of the electric field wave power measured by the Lang-
228 muir Probes and Waves (LPW) instrument (Andersson et al., 2015) in passive mode, the
229 normalized high energy electron pitch angle distribution, and the normalized low energy
230 electron pitch angle distribution, respectively, over a ~ 3 minute period. Note that 4b
231 and 4c have different color bar scales. The shape parameter is less than 1 in all direc-
232 tions (including trapped electrons) for this time period (photoelectrons dominate the low
233 energy distribution, see Xu et al. (2017) for details), indicating that these measurements
234 all took place on closed crustal field structures.

235 As altitude increases (right to left of Figures 4a, b, and c), the low energy electron
236 source cone becomes deeper, in agreement with the general trend of modeling results and
237 the statistical averages, from 04:07:50 - 04:06:45. The artificial diagonal line seen on top
238 of this natural source cone is due to sunlight contamination. The high energy electrons
239 have more noise than the lower energies and are isotropic. During this time period, the
240 magnetic elevation angle rotates from horizontal ($\sim 20^\circ$ at 04:07:50) to near-vertical ($\sim 80^\circ$ at
241 04:06:45). Around 04:06:45, the low energy electrons form a loss cone distribution, with
242 more flux away from the planet than toward. The low energy electrons then transition
243 into a slightly asymmetric source cone with more flux toward the planet than away from
244 04:06:30 - 04:06:40. At the same time, the high energy electrons have an intense flux in-
245 crease at perpendicular pitch angles. The full energy-pitch angle distribution at 04:06:33
246 (indicated by the dashed white line) is shown in Figure 4d, and the normalized energy
247 averaged PAD is displayed in Figure 4e (vertical slices through 4b,c). The exact values
248 do not match as different normalization factors are used between 4b,c and 4e. Through-
249 out these observations, LPW measured wave activity in the 2 - 30 Hz range. These fre-
250 quencies lie between the local ion (< 0.1 Hz) and electron gyrofrequency (> 1000 Hz)
251 for this time period. At higher altitudes (> 405 km), the high energy electrons again are
252 isotropic, the low energy electrons have a source cone distribution, and the magnetic el-
253 evation angle rotates from vertical $\sim 80^\circ$ at 04:06:45) to horizontal ($\sim 20^\circ$ at 04:05:10).

254 Coinciding with the acute flux increase of perpendicular high energy electrons is
255 a burst of electric field wave activity measured by LPW. Examining the magnetic field
256 reveals many fluctuations across this time period, however no distinct frequency stands
257 out when an FFT is performed. More analysis should be done on this time period to in-
258 vestigate the physics, but this is beyond the scope of this study and is left for future work.
259 The purpose of this example is to demonstrate that the 2-year statistical averages of low
260 and high energy PADs can be observed in any given observation.

261 6 Discussion & Conclusion

262 One process that could form the distributions observed for high energy photoelec-
263 trons is magnetic pumping (Borovsky, 1986). Magnetic pumping is the result of two dif-
264 ferent waves effects on a particle population. A compressional magnetosonic wave will
265 compress and relax the plasma due to ExB drift provided the frequency of the wave is

266 small such that the first adiabatic invariant is conserved. If another wave (in cyclotron
267 resonance with the particles) is also present and is actively pitch angle scattering the par-
268 ticle population, then the compression/relaxation cycle of the particles is interrupted and
269 particles may gain energy from the compressional wave. At Mars, the compressional waves
270 could come from pressure variations in the solar wind, causing the crustal fields to com-
271 press and relax. Weber et al. (2019) recently observed that during periods of high so-
272 lar wind pressure, statistically, closed fields are seen less often and draped fields are seen
273 more often than during periods of low solar wind pressure. Due to the locality of the crustal
274 fields, a local time effect is expected to be observed if magnetic pumping is the domi-
275 nant process. A crustal field recently rotated onto the dayside will have experienced no
276 pumping during night and no perpendicular peak should exist. In contrast, a crustal field
277 on the dusk side will have experienced magnetic pumping throughout the day and the
278 effects should be maximized. No local time effect can be seen in the data (Figure S1),
279 and therefore we do not expect this to be the dominant process affecting the high en-
280 ergy electron pitch angle distributions.

281 Another process that could produce the observed distributions of high energy pho-
282 toelectrons on dayside closed crustal field lines is adiabatic heating due to cross field drifts.
283 On closed field lines, the gradient-curvature drift will be azimuthal, not radial, and would
284 therefore not typically move electrons into regions of higher field strength. Provided the
285 motional electric field and crustal field lines are in the correct orientation, solar wind elec-
286 trons can ExB drift across field lines and onto a closed crustal field structure. However,
287 Figures 2 and 3 are two year average distributions, and the angle between any individ-
288 ual crustal field line and the motional electric field is not constant enough for ExB drift
289 to be the dominant process to form the flux peak at perpendicular pitch angles. Although
290 a magnetosheath or external source of electrons can explain both the altitude dependence
291 and the asymmetry in fluxes with respect to the planet, it seems unlikely this is the domi-
292 nant mechanism due to two issues. First, there is a lack of a supply mechanism to the
293 closed crustal field line, though wave-particle interactions in the sheath may scatter par-
294 ticles onto closed field lines. Secondly, the pitch angle distributions of high energy elec-
295 trons on deep closed field lines ($|B| > 50nT$, $B_{elev} < 45^\circ$, and altitude > 400 km to
296 minimize collisional effects) still exhibit a perpendicular peak. Furthermore, whatever
297 mechanism would be supplying external electrons would need to be local time indepen-
298 dent as the perpendicular peak is seen immediately on the dawn side.

299 The most likely process that is producing the observed statistical distributions are
300 wave-particle interactions. Whistler mode waves are an example of an energy dependent
301 scattering mechanism and have recently been observed at Mars (Harada et al., 2016; Fowler
302 et al., 2018). These right-handed circularly polarized waves occur between the local ion
303 and electron gyrofrequency and will interact with different populations of electrons in
304 energy-pitch angle space depending on the background plasma conditions (thermal elec-
305 tron density and magnetic field magnitude) and on the wave parameters (wave frequency
306 and wave normal angle distributions). These waves can both pitch angle scatter and en-
307 ergy diffuse and are a good candidate process for producing the observed distributions.
308 While pitch angle scattering may be occurring, the dominant process seems to be ener-
309 gization of locally gyrating low energy electrons up to 100's of eV. Whistler waves are
310 capable of preferentially energizing these electrons. The example shown in Section 5 sup-
311 ports this explanation with both electric and magnetic variations observed between the
312 local ion and electron gyrofrequency, however it is by no means conclusive. Whistler mode
313 waves are generated when a temperature anisotropy occurs ($T_{e\perp} > T_{e\parallel}$). From a sin-
314 gle spacecraft pass, it is difficult to determine the location of wave generation, direction
315 of propagation, and region of interaction. For example, the increase in perpendicular flux
316 may have generated whistler waves instead of being the result of them, as was observed
317 by Fowler et al. (2018).

318 More work needs to be done in investigating the pitch angle distributions of superther-
 319 mal electrons on dayside closed crustal field lines at Mars. Statistical averages from MAVEN
 320 measurements show that low energy electrons behave as if collisional scattering and con-
 321 servation of the first adiabatic invariant are the only processes that control their distri-
 322 bution. High energy electrons on the other hand have an average distribution that can-
 323 not be explained by these two processes alone. A flux peak at perpendicular pitch an-
 324 gles indicates that a ubiquitous energization process is occurring on dayside closed crustal
 325 field lines with wave-particle interactions being the most likely candidate. It is difficult
 326 at the moment to explain the asymmetry with respect to the planet with wave-particle
 327 interactions. An external source of electrons can explain this, however this explanation
 328 suffers due to the lack of a supply mechanism. The modification of electron PADs at these
 329 high energies is of direct importance to the energy budget in the Martian space environ-
 330 ment. With ionization cross sections peaking at these energies for the main neutral species,
 331 this energization process may affect the ionosphere below. However, the energized elec-
 332 trons are outside the loss cone and low energy electrons may still dominate the electron
 333 impact ionization due to higher fluxes. This will be especially important on the night-
 334 side as trapped electrons on closed field lines live longer (Shane et al., 2016) and will be
 335 able to deposit their energy deeper into the nightside ionosphere. Furthermore, these re-
 336 sults show that there are unstudied physical processes occurring in the Martian space
 337 environment on dayside closed crustal field lines.

338 Acknowledgments

339 This work was supported by the National Aeronautics and Space Administration (NASA)
 340 grant NNX16AQ04G to the University of Michigan. The MAVEN project is funded by
 341 NASA through the Mars Exploration Program. All MAVEN data can be accessed through
 342 the Planetary Data System (<https://pds.nasa.gov/>).

343 References

- 344 Andersson, L., Ergun, R. E., Delory, G. T., Eriksson, A., Westfall, J., Reed, H.,
 345 ... Meyers, D. (2015). The Langmuir Probe and Waves (LPW) Instru-
 346 ment for MAVEN. *Space Science Reviews*, 195(1), 173–198. doi: 10.1007/
 347 s11214-015-0194-3
- 348 Borovsky, J. E. (1986). Magnetic pumping by magnetosonic waves in the presence of
 349 noncompressive electromagnetic fluctuations. *The Physics of Fluids*, 29(10),
 350 3245–3260. doi: 10.1063/1.865842
- 351 Brain, D. A., Lillis, R. J., Mitchell, D. L., Halekas, J. S., & Lin, R. P. (2007).
 352 Electron pitch angle distributions as indicators of magnetic field topology
 353 near Mars. *Journal of Geophysical Research: Space Physics*, 112(A9). doi:
 354 10.1029/2007JA012435
- 355 Coates, A. J., Tsang, S. M. E., Wellbrock, A., Frahm, R. A., Winningham, J. D.,
 356 Barabash, S., ... Crary, F. J. (2011). Ionospheric photoelectrons: Comparing
 357 Venus, Earth, Mars and Titan. *Planetary and Space Science*, 59(10), 1019–
 358 1027. doi: <https://doi.org/10.1016/j.pss.2010.07.016>
- 359 Connerney, J. E. P., Espley, J., Lawton, P., Murphy, S., Odom, J., Oliverson, R., &
 360 Sheppard, D. (2015). The MAVEN Magnetic Field Investigation. *Space Science*
 361 *Reviews*, 195(1), 257–291. doi: 10.1007/s11214-015-0169-4
- 362 Fowler, C. M., Andersson, L., Ergun, R. E., Harada, Y., Hara, T., Collinson, G., ...
 363 Jakosky, B. M. (2018). MAVEN Observations of Solar Wind-Driven Magne-
 364 tosonic Waves Heating the Martian Dayside Ionosphere. *Journal of Geophys-
 365 ical Research: Space Physics*, 123(5), 4129–4149. doi: 10.1029/2018JA025208
- 366 Frahm, R. A., Sharber, J. R., Winningham, J. D., Wurz, P., Liemohn, M. W.,
 367 Kallio, E., ... Mckenna-Lawler, S. (2006). Locations of Atmospheric Photo-
 368 electron Energy Peaks Within the Mars Environment. *Space Science Reviews*,

- 369 126(1), 389–402. doi: 10.1007/s11214-006-9119-5
- 370 Frahm, R. A., Winningham, J. D., Sharber, J. R., Scherrer, J. R., Jeffers, S. J.,
371 Coates, A. J., . . . Dierker, C. (2006). Carbon dioxide photoelectron en-
372 ergy peaks at Mars. *Icarus*, 182(2), 371–382. doi: [https://doi.org/10.1016/](https://doi.org/10.1016/j.icarus.2006.01.014)
373 [j.icarus.2006.01.014](https://doi.org/10.1016/j.icarus.2006.01.014)
- 374 Harada, Y., Andersson, L., Fowler, C. M., Mitchell, D. L., Halekas, J. S., Mazelle,
375 C., . . . Jakosky, B. M. (2016). MAVEN observations of electron-induced
376 whistler mode waves in the Martian magnetosphere. *Journal of Geophysical*
377 *Research: Space Physics*, 121(10), 9717–9731. doi: 10.1002/2016JA023194
- 378 Itikawa, Y. (2002). Cross Sections for Electron Collisions With Carbon Diox-
379 ide. *Journal of Physical and Chemical Reference Data*, 31(3), 749–767. doi:
380 10.1063/1.1481879
- 381 Jakosky, B. M., Lin, R. P., Grebowsky, J. M., Luhmann, J. G., Mitchell, D. F.,
382 Beutelschies, G., . . . Zurek, R. (2015). The Mars Atmosphere and Volatile
383 Evolution (MAVEN) Mission. *Space Science Reviews*, 195(1), 3–48. doi:
384 10.1007/s11214-015-0139-x
- 385 Khazanov, G. V., & Liemohn, M. W. (1995). Nonsteady state ionosphere-
386 plasmasphere coupling of superthermal electrons. *Journal of Geophysical*
387 *Research: Space Physics*, 100(A6), 9669–9681. doi: 10.1029/95JA00526
- 388 Khazanov, G. V., Liemohn, M. W., Gombosi, T. I., & Nagy, A. F. (1993). Non-
389 steady-state transport of superthermal electrons in the plasmasphere. *Geophys-*
390 *ical Research Letters*, 20(24), 2821–2824. doi: 10.1029/93GL03121
- 391 Liemohn, M. W., Frahm, R. A., Winningham, J. D., Ma, Y., Barabash, S., Lundin,
392 R., . . . Dierker, C. (2006). Numerical interpretation of high-altitude photo-
393 electron observations. *Icarus*, 182(2), 383–395. doi: [https://doi.org/10.1016/](https://doi.org/10.1016/j.icarus.2005.10.036)
394 [j.icarus.2005.10.036](https://doi.org/10.1016/j.icarus.2005.10.036)
- 395 Liemohn, M. W., Mitchell, D. L., Nagy, A. F., Fox, J. L., Reimer, T. W., & Ma,
396 Y. (2003). Comparisons of electron fluxes measured in the crustal fields at
397 Mars by the MGS magnetometer/electron reflectometer instrument with a
398 B field-dependent transport code. *Journal of Geophysical Research: Planets*,
399 108(E12). doi: 10.1029/2003je002158
- 400 Mitchell, D. L., Mazelle, C., Sauvaud, J.-A., Thocaven, J.-J., Rouzaud, J., Fedorov,
401 A., . . . Jakosky, B. M. (2016). The MAVEN Solar Wind Electron Analyzer.
402 *Space Science Reviews*, 200(1), 495–528. doi: 10.1007/s11214-015-0232-1
- 403 Shane, A. D., Xu, S., Liemohn, M. W., & Mitchell, D. L. (2016). Mars nightside
404 electrons over strong crustal fields. *Journal of Geophysical Research: Space*
405 *Physics*, 121(4), 3808–3823. doi: 10.1002/2015JA021947
- 406 Thompson, W. R., Shah, M. B., & Gilbody, H. B. (1995). Single and double ion-
407 ization of atomic oxygen by electron impact. *Journal of Physics B: Atomic,*
408 *Molecular and Optical Physics*, 28(7), 1321–1330. doi: 10.1088/0953-4075/28/
409 7/023
- 410 Weber, T., Brain, D., Mitchell, D., Xu, S., Connerney, J., & Halekas, J. (2017).
411 Characterization of Low-Altitude Nightside Martian Magnetic Topology Using
412 Electron Pitch Angle Distributions. *Journal of Geophysical Research: Space*
413 *Physics*, 122(10), 9777–9789. doi: 10.1002/2017JA024491
- 414 Weber, T., Brain, D., Mitchell, D., Xu, S., Espley, J., Halekas, J., . . . Jakosky,
415 B. (2019). The Influence of Solar Wind Pressure on Martian Crustal Mag-
416 netic Field Topology. *Geophysical Research Letters*, 46(5), 2347–2354. doi:
417 10.1029/2019GL081913
- 418 Xu, S., Liemohn, M., Bougher, S., & Mitchell, D. (2016). Martian high-altitude pho-
419 toelectrons independent of solar zenith angle. *Journal of Geophysical Research:*
420 *Space Physics*, 121(4), 3767–3780. doi: 10.1002/2015JA022149
- 421 Xu, S., & Liemohn, M. W. (2015). Superthermal electron transport model for Mars.
422 *Earth and Space Science*, 2(3), 47–64. doi: 10.1002/2014EA000043
- 423 Xu, S., Liemohn, M. W., & Mitchell, D. L. (2014). Solar wind electron precipitation

- 424 into the dayside Martian upper atmosphere through the cusps of strong crustal
425 fields. *Journal of Geophysical Research: Space Physics*, 119(12), 10,100–
426 110,115. doi: 10.1002/2014JA020363
- 427 Xu, S., Mitchell, D., Liemohn, M., Fang, X., Ma, Y., Luhmann, J., . . . Jakosky, B.
428 (2017). Martian low-altitude magnetic topology deduced from MAVEN/SWEA
429 observations. *Journal of Geophysical Research: Space Physics*, 122(2), 1831–
430 1852. doi: 10.1002/2016JA023467
- 431 Xu, S., Thiemann, E., Mitchell, D., Eparvier, F., Pawlowski, D., Benna, M., . . .
432 Mazelle, C. (2018). Observations and Modeling of the Mars Low-Altitude Iono-
433 spheric Response to the 10 September 2017 X-Class Solar Flare. *Geophysical*
434 *Research Letters*, 45(15), 7382–7390. doi: 10.1029/2018GL078524
- 435 Xu, S., Weber, T., Mitchell, D. L., Brain, D. A., Mazelle, C., DiBraccio, G. A., &
436 Espley, J. (2019). A Technique to Infer Magnetic Topology at Mars and Its
437 Application to the Terminator Region. *Journal of Geophysical Research: Space*
438 *Physics*, 124(3), 1823–1842. doi: 10.1029/2018JA026366

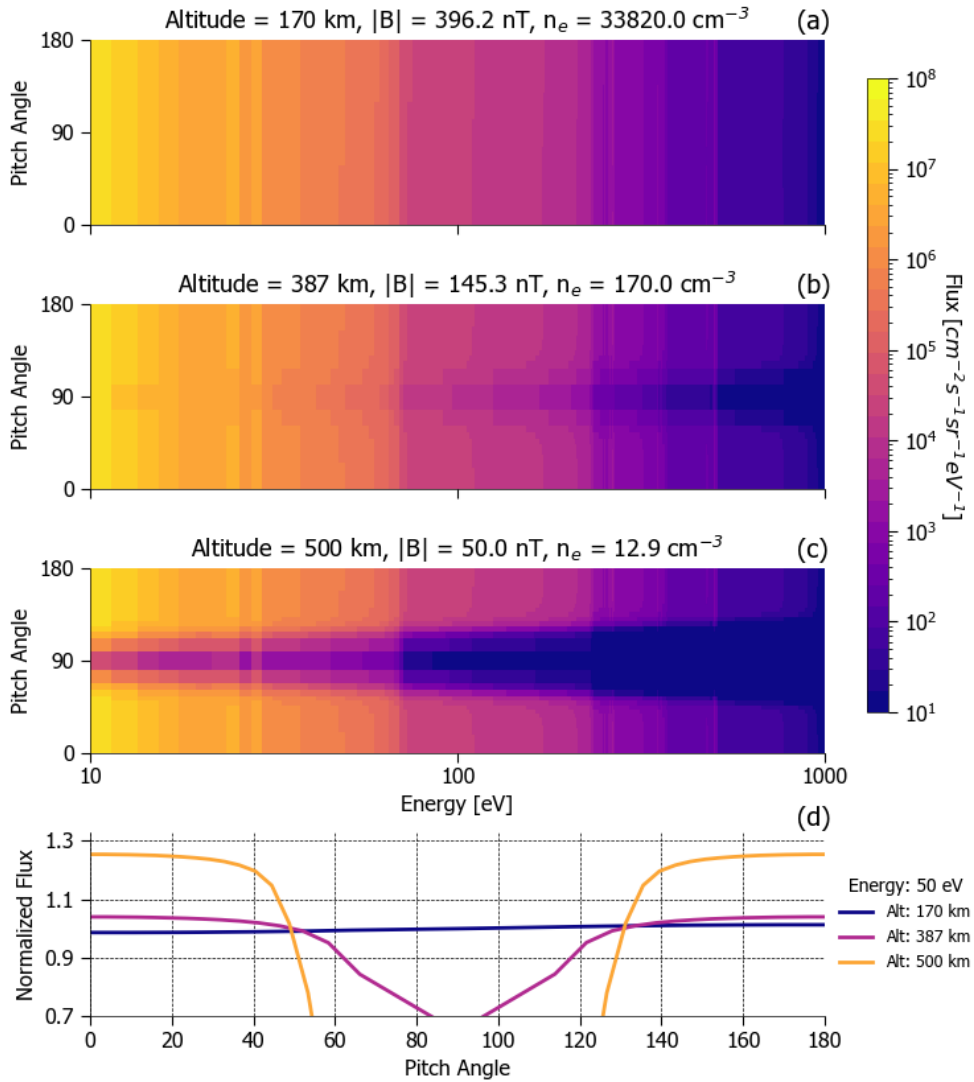


Figure 1. Superthermal electron transport (STET) model results of photoelectron pitch angle distributions at three representative locations along a crustal dipole-like magnetic field line: (a) near the exobase, (b) above the exobase, and (c) at the top of the field line. (d) Normalized pitch angle distributions for electrons with energy = 50 eV at each altitude.

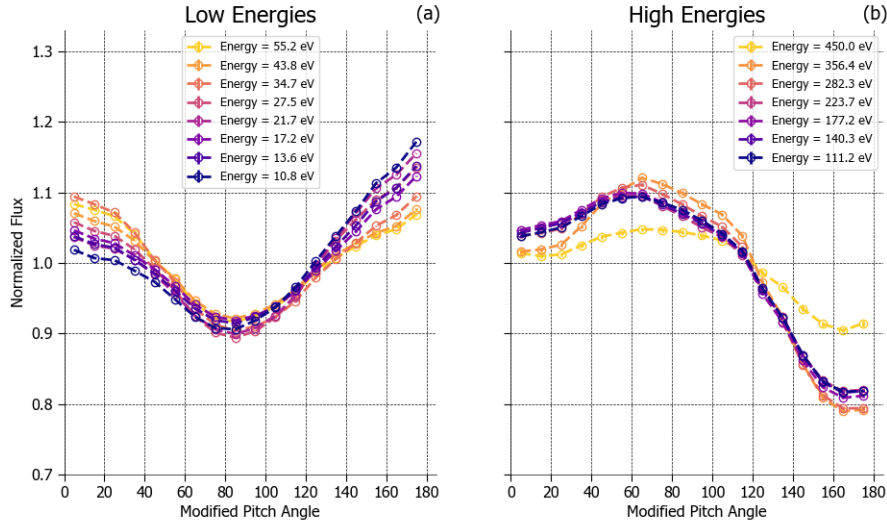


Figure 2. Normalized pitch angle distributions of photoelectrons for (a) low and (b) high energies. The error bars include both measurement and statistical sources of error and are contained within each data marker.

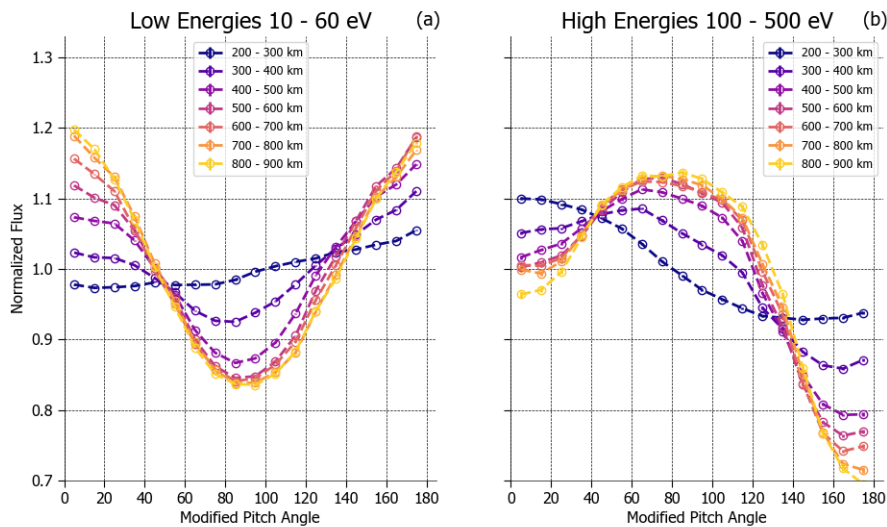


Figure 3. Normalized pitch angle distributions of (a) low and (b) high energy photoelectrons as a function of altitude. The error bars include both measurement and statistical sources of error and are contained within each data marker.

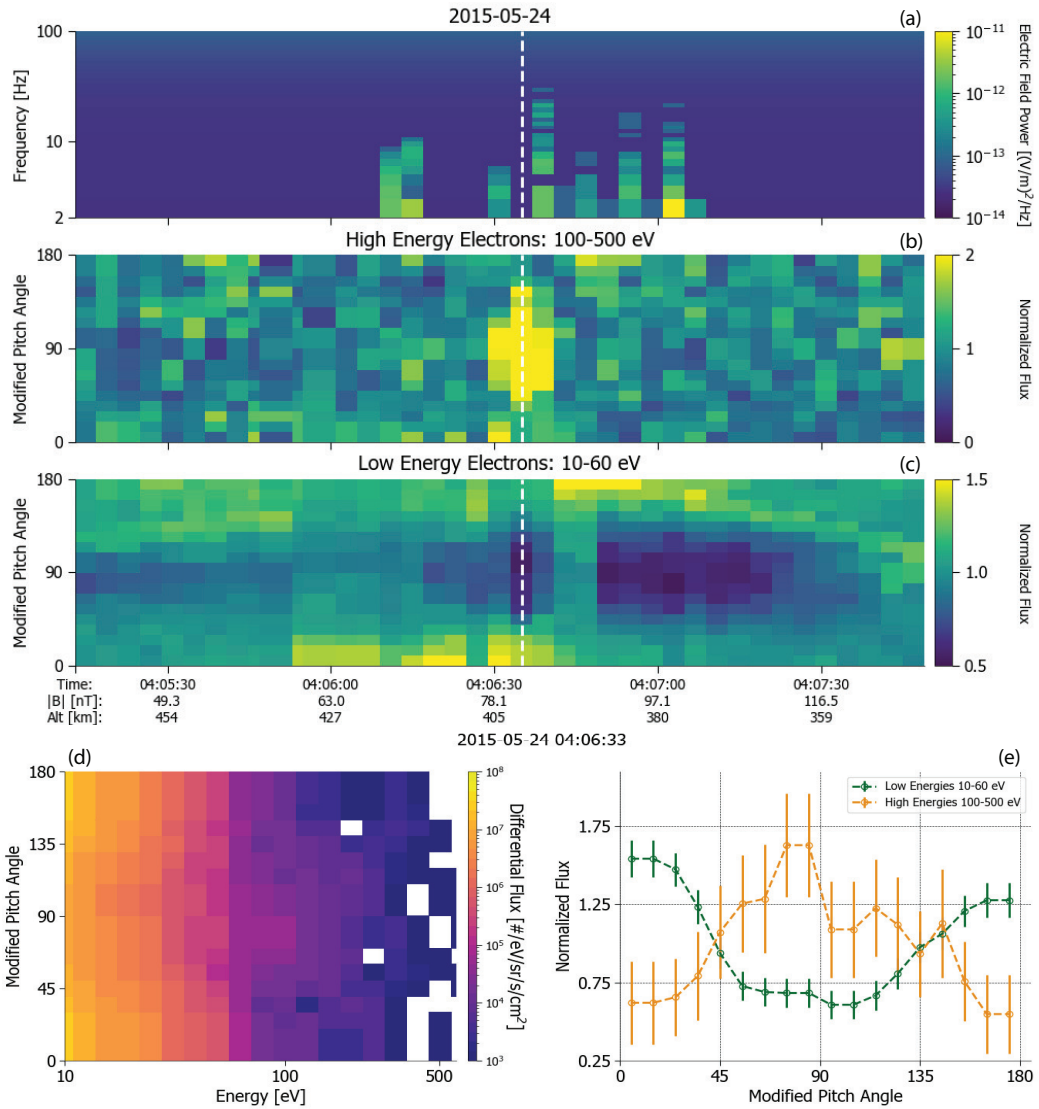
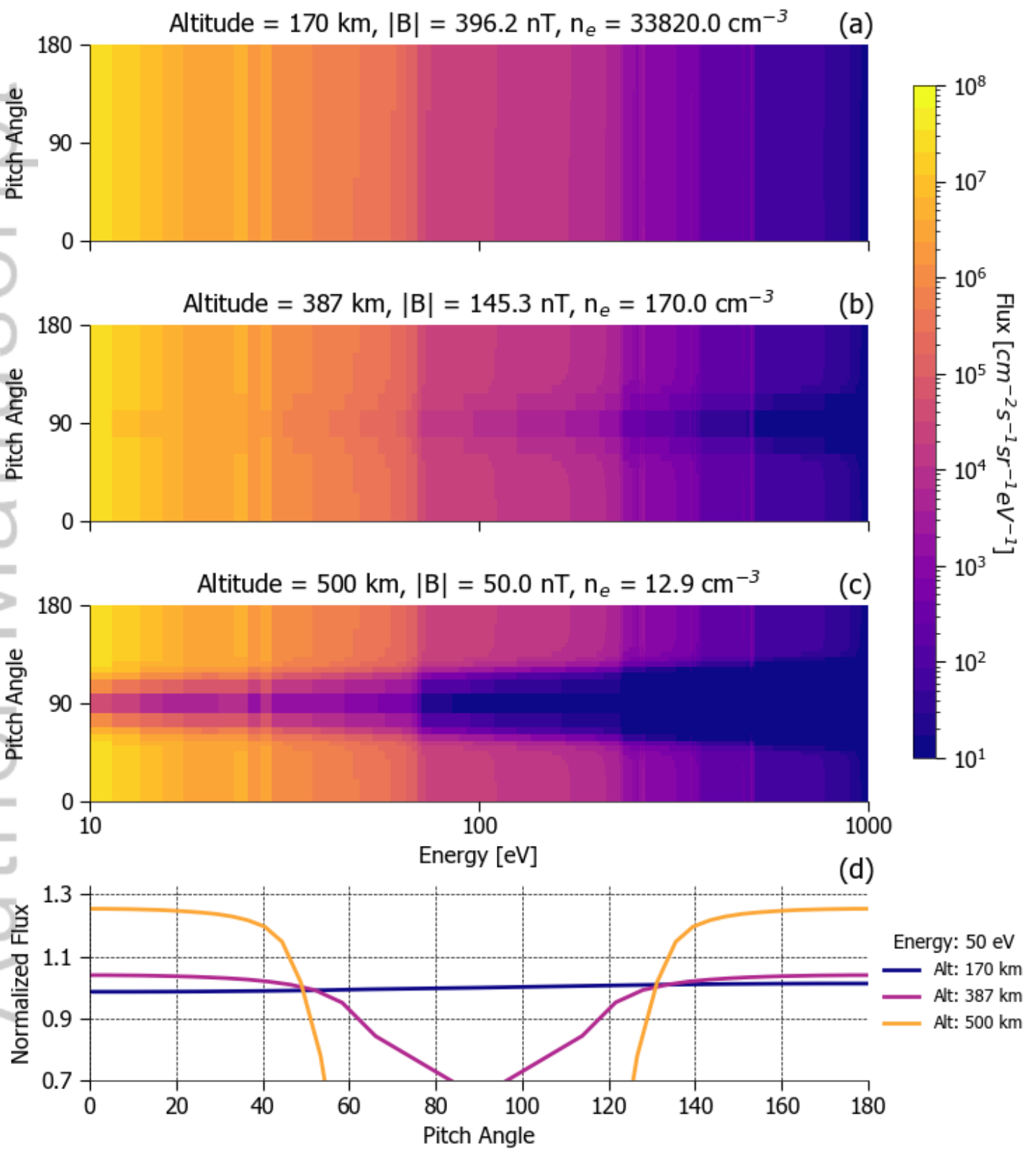
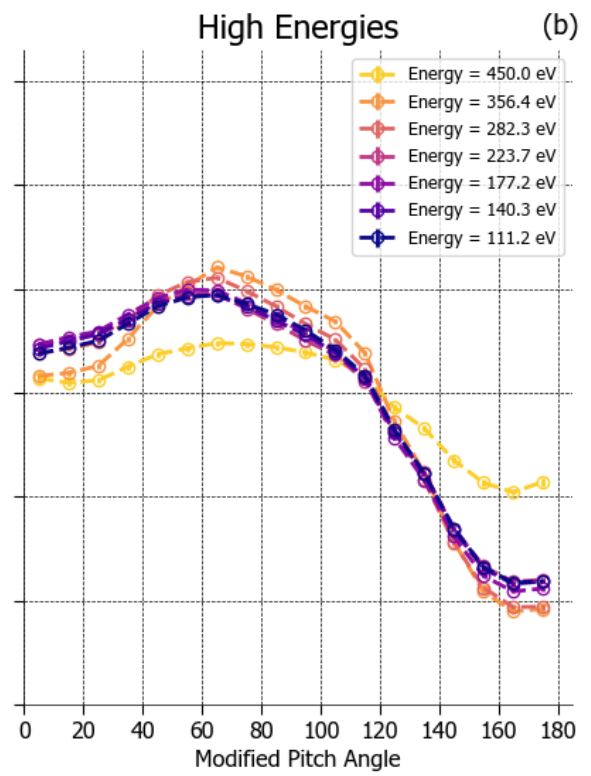
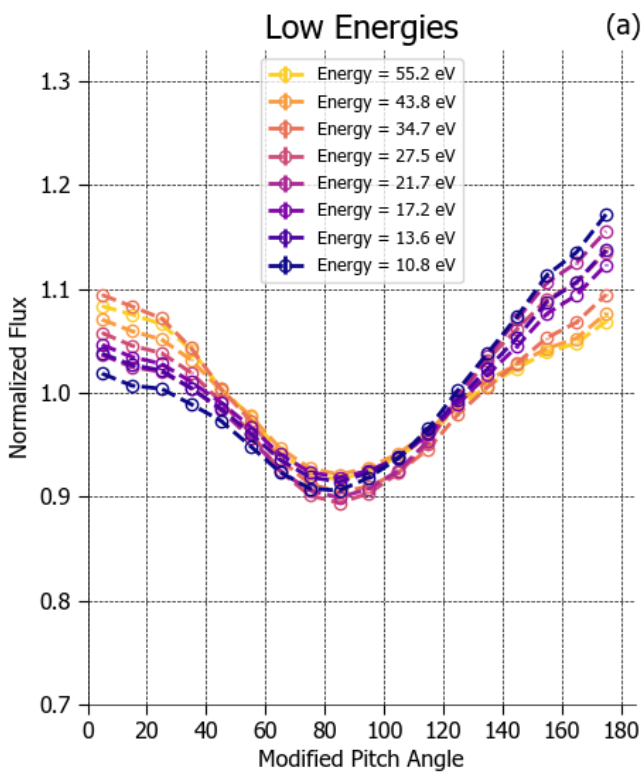
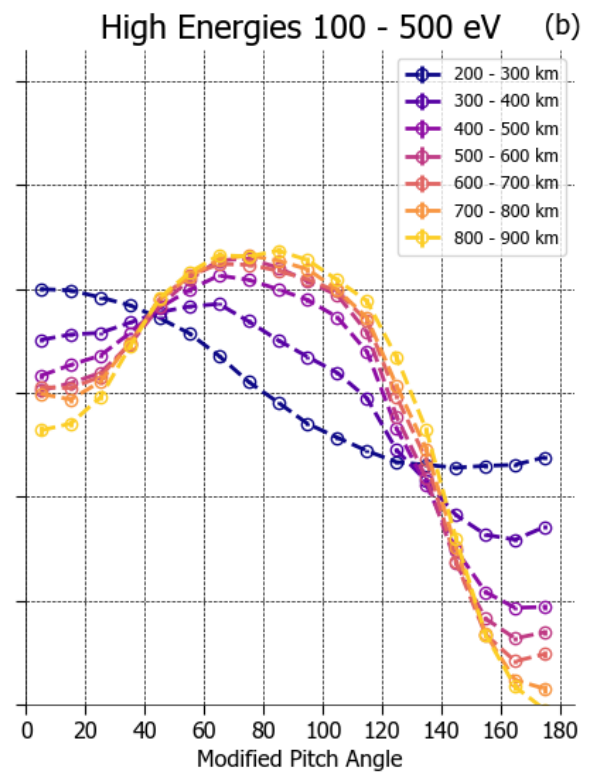
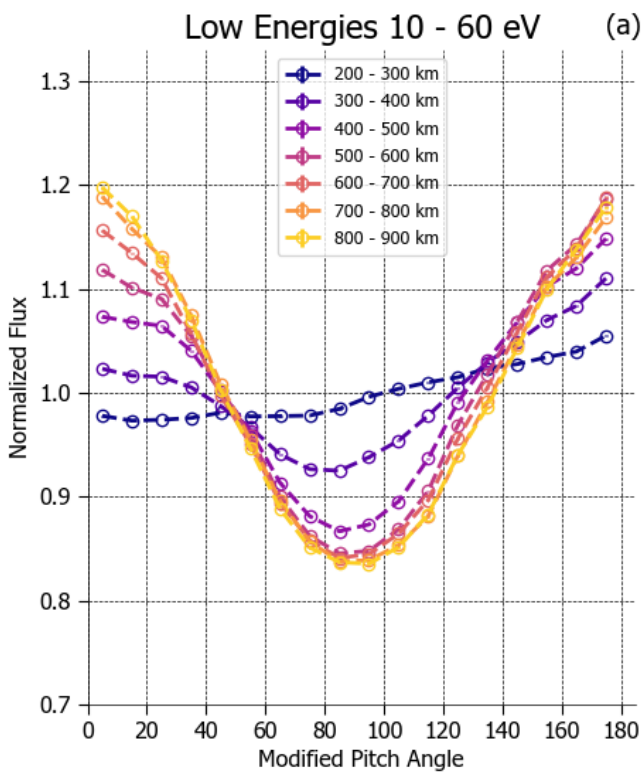


Figure 4. Time series of (a) electric wave power spectra from the Langmuir Probes and Waves (LPW) instrument, (b) normalized high energy photoelectron pitch angle distributions, and (c) normalized low energy photoelectron pitch angle distributions. The white dashed line marks the observation at 04:06:33 with the complete energy-pitch angle distribution at this time shown in (d) and the normalized energy-averaged pitch angle distributions shown in (e).

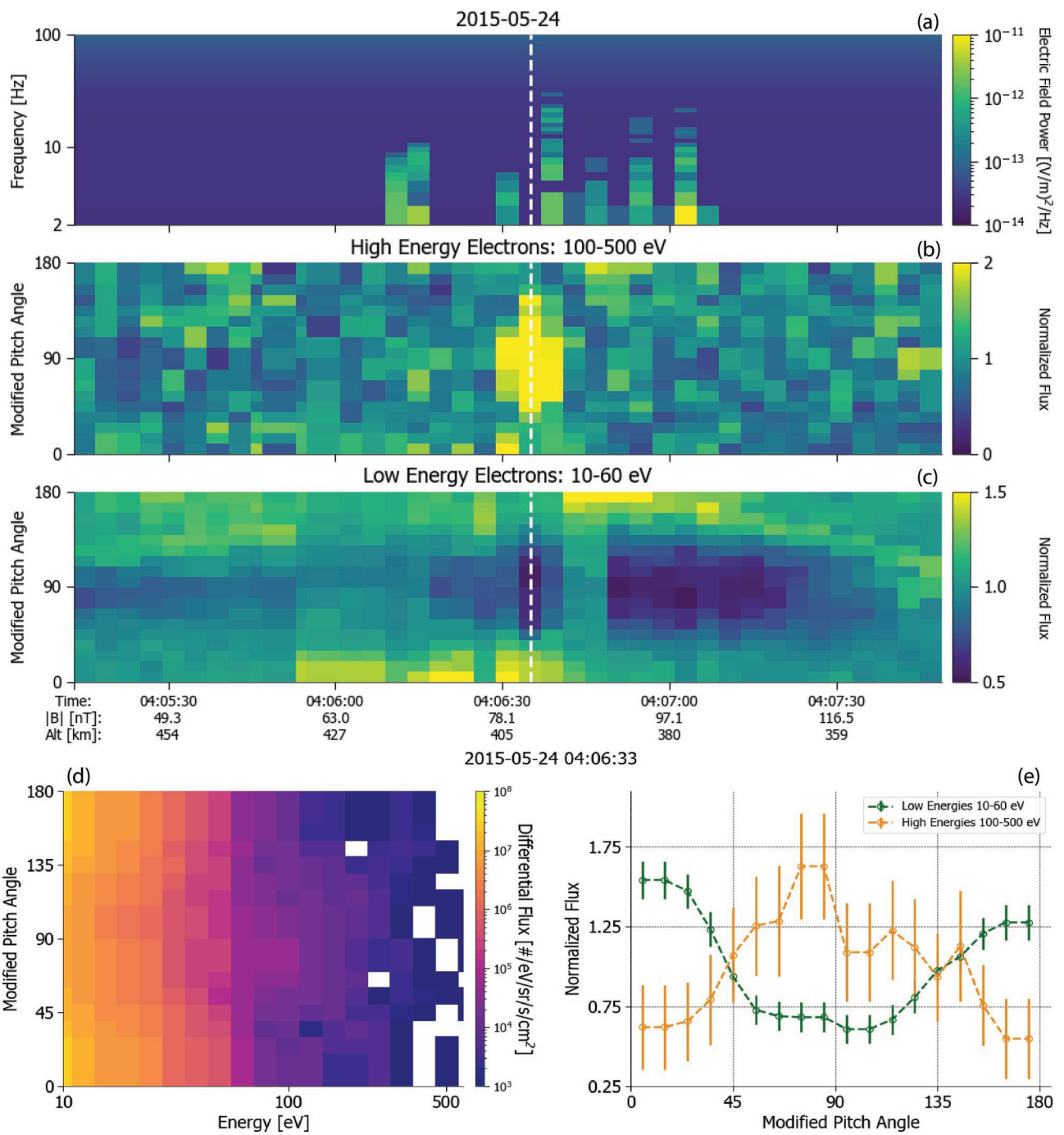




2019GL084919-f02-z-.png



2019GL084919-f03-z-.png



2019gl084919-f04-z-.eps